Manuscript published in
Fire Safety Journal, 2009, Vol. 44, pp. 779–788

Contribution to flashover modelling: Development of a validated numerical model for ignition of non-contiguous wood samples

Andrej Horvat[1], Yehuda Sinai
Anthony Pearson and Jean-Michel Most

Abstract

A computational model of flashover is presented that closely follows the experimental setup at CNRS-ENSMA-Poitiers. A propane burner with thermal power of 55 kW is used as a primary source of fire and square beech wood samples (30 mm × 30 mm × 5 mm) as fire spread targets. The computational model describes the wood pyrolysis with a progress variable. Using the conservation of heat fluxes at the solid-gas interface, the thermal diffusion in the wood samples is coupled with the convective and the radiative heat transfer in the ambient gas phase. The incoming heat flux at the upper surface of the wood samples reaches values between 20 and 30 kW/m^2. With the ignition and subsequent combustion of the pyrolysis volatiles, the heat flux increases by approx. 12 kW/m^2. The results show that the ignition of the wood samples is triggered at an approx. surface temperature of 650 K. Due to large local variations in incident heat flux, significant differences in the ignition times of the wood samples are observed. The comparison of the calculated and the experimentally measured temperature shows a good agreement for the first wood sample and the model predicts the ignition time very well. But for the second and the third wood samples the model overpredicts the temperature, which leads to a premature ignition of these wood samples.

[1] Corresponding author

Nomenclature

Latin letters

A_p	pre-exponential factor of the pyrolysis reaction
c_p	specific heat
C_A	Eddy dissipation model parameter
D	molecular diffusivity
E_p	activation energy of the pyrolysis reaction
f	mass flux
F_1 , F_2	SST model blending functions
g	gravitational acceleration
G	turbulence production term due to buoyancy
h	enthalpy
I	radiation intensity
k	thermal conductivity, turbulence kinetic energy
k_g , k_{HCg}	empirical parameters of the radiation model
K	radiation coefficient
ℓ	wall distance
m	mass flow
M	molar mass
p	pressure
P	turbulence production term due to stresses
Pr_t	turbulent Prandtl number (= 0.9)
q	heat flux
r	spatial dependence
R	gas constant, reaction rate

s	ray path length
S	source term, surface, invariant of the strain rate
Sc_t	turbulent Schmidt number (= 0.9)
t	time
T	temperature
v	velocity
V	volume
x, y, z	spatial coordinates

Greek letters

α	progress variable of the pyrolysis reaction, heat transfer coefficient
α_1, α_3	SST model parameter
β^*, β_3	SST model parameters
δ	Kronecker delta function, wall thickness
ε	emissivity, turbulence eddy dissipation
ζ	molecular concentration
θ	angle
λ	wave length
μ	dynamic viscosity
ν	stoichiometric coefficients
ξ	mass fraction
ρ	density
$\sigma_{\omega 2}$, σ_{k3}, $\sigma_{\omega 3}$	SST model parameters
Ψ	volume fraction
φ	angle

Ω	angle
ω	turbulence frequency

Subscripts/superscripts

0	starting radiation intensity
a	absorption
b	blackbody
b_{1g} , b_{2g}	radiation model parameters
c	char, component, convection
comb	combustion
g	gaseous phase
i	irradiation
insul	insulation
p	pyrolysis
rad	radiation
ref	reference state
s	solid, scatter
stat	static
t	turbulence
v	volatiles
w	wood

Symbols

′	fluctuation from a time average
–	time average

1 Introduction

A fire in a confined space can be divided into three distinct stages based on fuel and oxygen consumption, heat release and variation of average gas temperature. These stages are usually described as the fire growth period, fully developed fire and decay period. Flashover is a short period of transition from a localized initial fire to the fully developed fire where all fuel surfaces within the compartment start to burn [1]. During the pre-flashover stage, the fire develops from its origin, forming a hot layer of combustion products below the ceiling of the enclosure. Thermal radiation from the fire and the hot layer raises the surface temperature of the surrounding combustible material. The material starts to pyrolyse [2] releasing volatiles that may ignite. The ignition of the combustible volatiles results in a rapid flame spread from a localized fire to all combustible surfaces. A more detailed description of this phenomenon may be found in [1], [3] and [4].

From the fire-fighting perspective, flashover is a critical stage of fire growth. Namely, when flashover takes place, the probability of survival of occupants rapidly decreases. As the transition from the initial localized fire to the general conflagration takes usually less than a minute [5], fatalities are very likely to occur. Also, flashover creates a large increase in the rate of combustion; therefore, significantly greater effort is needed to reduce the burning material below its ignition temperature [6].

Due to the hazard associated with flashover, the subject has received a fair amount of attention in the literature. Drysdale [1] collected probably the most comprehensive overview of experimental studies. More recent analysis of flashover experimental data can be found in [5] and [7]. Although, the emphasis of this paper is on computational modelling of flashover, it is also important to mention a full-scale experiment conducted by White et al. [8], where a

train fire was allowed to become fully developed, involving all combustible materials within the train.

Computational models used to analyse flashover can be classified into zone and field models. The theoretical background of zone models is the conservation of mass and energy in a compartment fire. The simulation domain is divided into separate zones and the conditions in each zone are assumed to be constant. Most often the fire is described with two-zones (lower cold layer and upper hot layer). As such description of a complex phenomenon is rather coarse, zone models have to incorporate empirical observations regarding fire dynamics and smoke movement. Some of the applications of zone models to flashover scenario were published by Spearpoint et al. [4], Lou et al. [9], and Chow [10]. More recently, Novozhilov [11] presented an analysis of flashover development under fire suppression conditions using a zone model.

In comparison to zone models, field models offer much larger modelling flexibility due to local, Eulerian field description of physical variables. Initial applications of field models to fire spread over solid surfaces were published by Atreya [12] and Fredland [13]. Nevertheless, a numerical prediction of transient behaviour of flashover that incorporates flow dynamics, convective and radiation heat transfer, thermal and chemical decomposition of solid material is still a challenging task. Although, more recent applications [9, 14, 15] show better prediction of magnitude and trends during flashover, large discrepancies in comparison to experimentally obtained values still exist [16].

The present paper describes an experimental investigation conducted by the group at CNRS-ENSMA-Poitiers and modelling work performed by ANSYS Europe Ltd. The motivation behind the experimental work was to re-create a situation similar to flashover in a controllable

(and repeatable) laboratory environment. The experiments contain all the elements of flashover although on a much smaller (and less hazardous) scale. The experimental data were obtained for a thick solid material in order to validate the developed mathematical model.

Using a comparison of the collected experimental and simulation results, the paper discusses the suitability of the considered modelling technique to predict flashover, analyses weaknesses of the model and gives recommendations for further development.

2 Description of the experiment

Five experiments were performed under identical conditions to get a representative set of results. In these experiments a primary fuel source – a gas burner – was located in a zone of fresh air underneath a hood. A fire plume is generated above the burner and reaches into the hood, generating a zone of vitiated gas and soot. The distance between the burner and the hood was set so that insufficient air is entrained into the plume. Sufficient fuel is transported into the upper layer for the gas mixture to be fuel rich. As a consequence, combustion at the interface between the smoke zone and the fresh air below is sustained. A photograph of the installation is given in Figure 1.

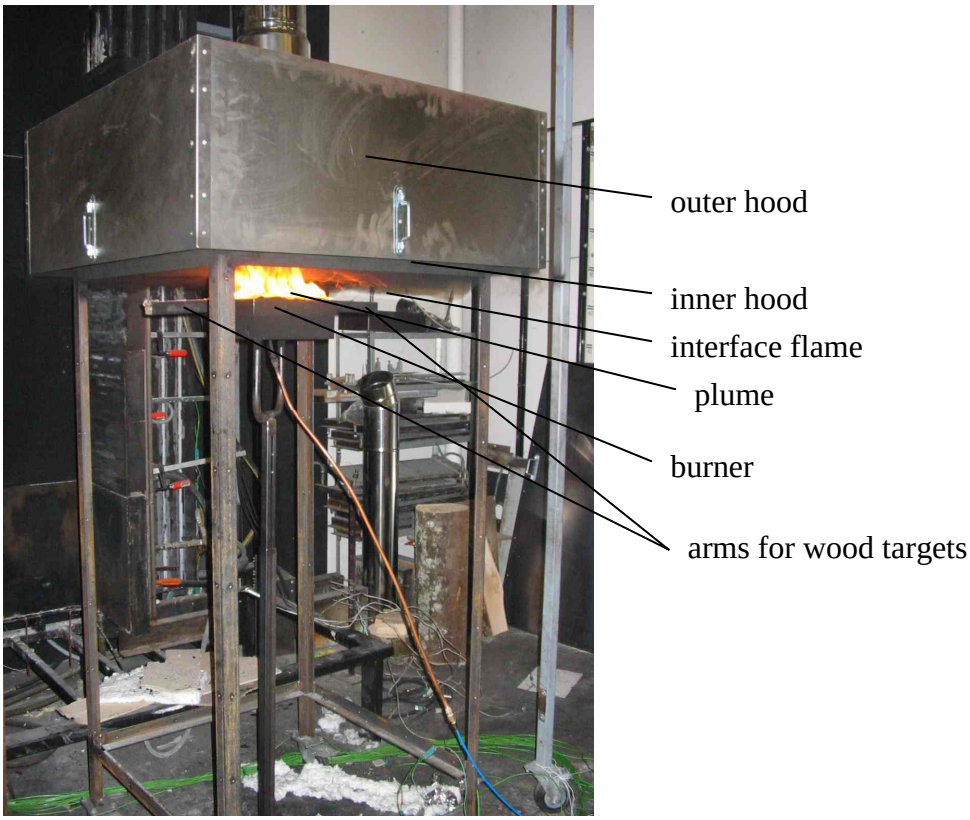

Figure 1: Photograph of the installation during one of the tests

The primary fuel source was a sand burner measuring 0.25 m square by 0.10 m depth. The burner was placed on the vertical axis of the hood, with its upper surface located 0.05 m below the height of the lower edge of the hood. The burner was supplied with propane through a mass flow regulator. The regulator was set to provide a fuel flow rate of 1.2 g/s, which equates to a thermal power of approximately 55 kW.

The tests were performed under a double-walled hood. The hood was designed so that smoke which spills out from underneath the inner hood is captured in the outer hood and led to a chimney, allowing measurements of the composition of the gases. The internal measurements of the inner hood were: length and width 0.76 m, depth 0.27 m. The inner hood was made from 2 mm thick steel sheets, with lining of mineral fibreboard – 25 mm thick on the ceiling,

20 mm on the walls. The outer hood measured 1 m square, by 0.4 m deep and was made from 2 mm thick steel sheets. The dimensions (in mm) are given in Figure 2.

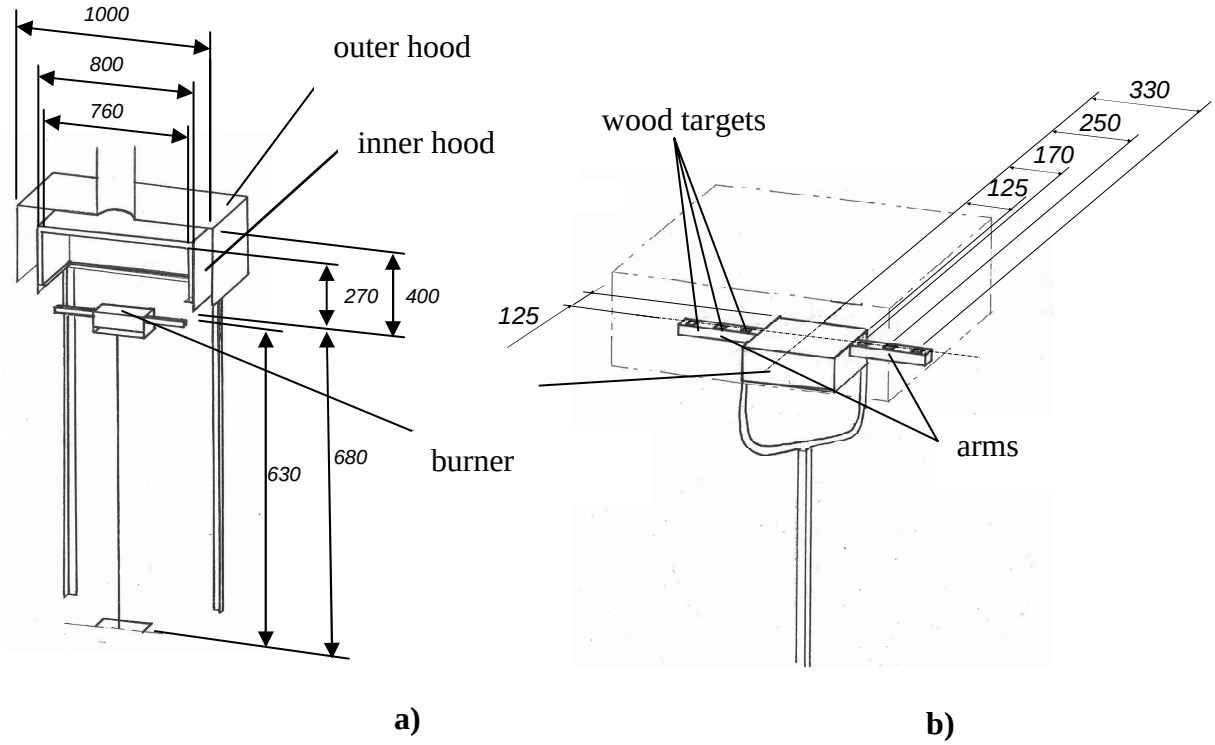

Figure 2: Schematic overview: **a)** gas burner, inner and outer hood, **b)** geometry of the gas burner and secondary fuel sources

Three blocks of beech wood were placed on each arm radiating out from the sides of the burner. They were located at the same height as the surface of the burner, 0.17 m, 0.25 m and 0.33 m, respectively from the vertical axis of the burner to the centre of the target. The arms were packed with mineral fibre insulation board, so the sides and underside of the wood samples were covered with mineral fibre. The blocks were subject to heat transfer from the plume, the interface flame, the smoke layer, and the walls, so that the total heat flux was sufficient for the objects to undergo non-piloted ignition. In order to minimize variation of the behaviour, the size of the exposed surface of the wood samples was kept small – specifically 30 mm × 30 mm. The thickness of the targets was 5 mm.

The non-piloted ignition observed in experiments can be interpreted as the onset of the flashover event. The non-contiguous wood targets were used to observe the difference in ignition time. In the real flashover scenario this may be equivalent to multiple (non-contiguous) pieces of furniture, which will have different ignition time based on their location in a room. As such, the conducted experiments represent most of the physics of flashover at its early stage, when the fire dynamics is not limited by the space and ventilation conditions.

More detailed description of the experimental tests is given in [17].

3 Mathematical modelling

The numerical model closely follows the experimental test section [17]. As symmetrical behaviour is expected, only half of the experimental domain is modelled in order to reduce computational requirements (Fig. 3). The double hood arrangement is simplified and modelled as a single hood. The exhaust that collected smoke during the experiments is not taken into account. The dimensions of the simulation domain that encloses the burner and the hood are 0.76 m in x, 1.52 m in y, and 0.9 m in z direction.

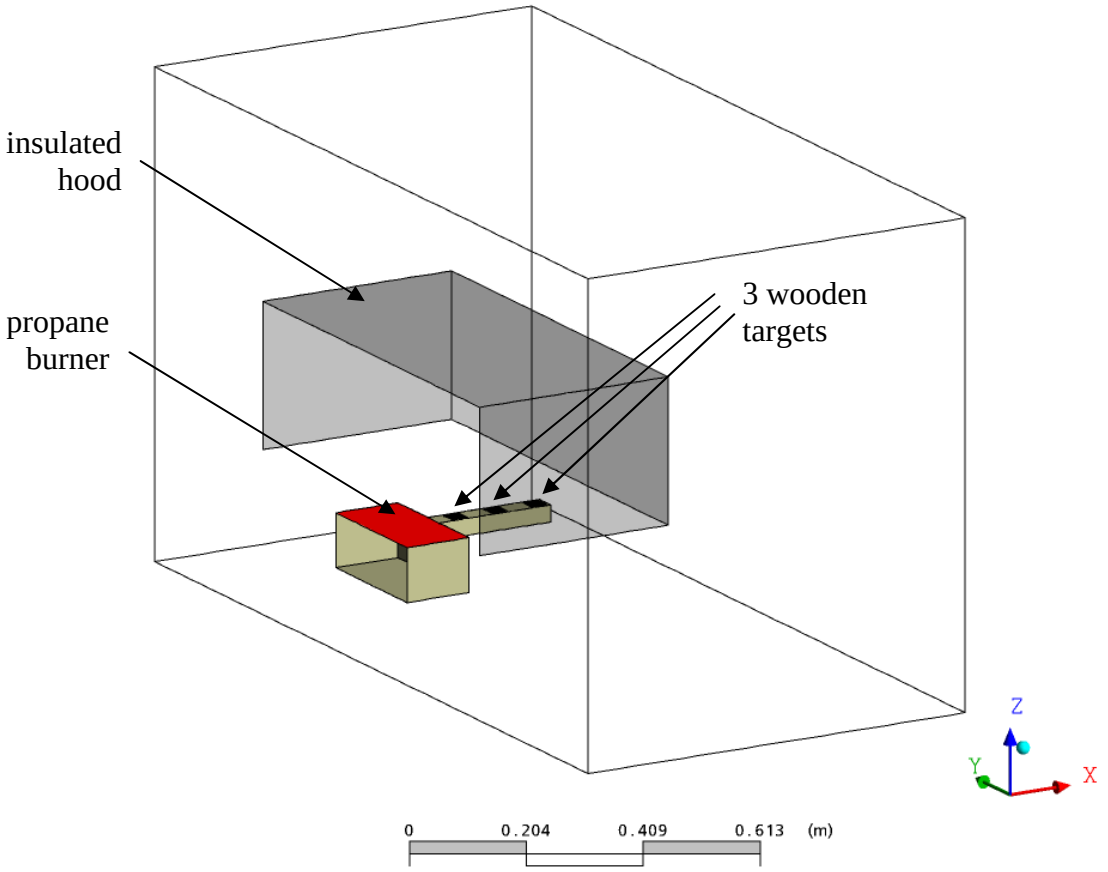

Figure 3: Numerical simulation domain of the CFD model

The applied numerical model of flashover describes transport of mass, momentum and energy in gaseous environment. It also includes combustion and thermal radiation. As the same time, degradation of wood samples is described with a pyrolysis model.

3.1 Pyrolysis model

In the numerical model, pyrolysis of wood was approximated with a single stage chemical reaction:

$$wood \rightarrow \nu_c\, char + volatiles \quad (1)$$

The pyrolysis front is tracked with a progress variable that defines a solid mixture of virgin wood and char as proposed by Novozhilov et al. [18]:

$$\rho_s = \rho_w \alpha + \rho_c (1-\alpha) \ . \tag{2}$$

As well as the transport equation for the progress variable α:

$$\partial_t \rho_s = -(\rho_w \alpha) A_p \, exp\left(-\frac{E_p}{RT}\right) \ , \tag{3}$$

the energy transport equation for the solid mixture static enthalpy is solved as

$$\partial_t (\rho_s h_s) + \partial_i (f_g h_g) = \partial_i (k_s \, \partial_i T) + \Delta h_p \partial_t \rho_s \ , \tag{4}$$

where the second term represents heat convection due to volatiles. In order to calculate mass fluxes of volatiles f_g, a transport equation for solid mixture

$$\partial_t \rho_s + \partial_i f_g = 0 \tag{5}$$

is integrated over the volume V:

$$f_g(z) = -\frac{1}{S_o} \int_V \partial_t \rho_s \ d\Omega \quad . \tag{6}$$

Material properties used in both tested models were taken from [12], [13] and [19]. They are summarized in Table 1.

Table 1: Material properties and reaction kinetics constants for the pyrolysis models

	wood	char
Molar mass, M [kg kmol^{-1}]	94.0	12.0
Density, ρ [kg m^{-3}]	730.0	182.5
Thermal conductivity, k [W m^{-1} K^{-1}]	0.3	0.42
Specific heat, c_p [J kg^{-1} K^{-1}]	1500.0	1300.0
Emissivity, ε [-]	0.6	1.0
Heat of pyrolysis, Δh_p [kJ kg^{-1}]	430.0	
Pre-exponential factor, A_p [s^{-1}]	4.37e9	
Activation energy, E_p [J mol^{-1}]	1.43e5	

Approximately 75 % of the wood mass is converted into volatiles, parts of which are combustible gases: H_2, CO, CH_4 and higher hydrocarbons:

$$volatiles \rightarrow \nu_g \; gas + residual \quad . \tag{7}$$

Their total heat release rate is approximated with an equivalent mass flow of a single gas; in the present model, this is methane. By comparing the combustion heat of wood [20] with the heat of combustion of methane

$$m_w \Delta h_w^{comb} = m_{\mathrm{CH_4}} \Delta h_{\mathrm{CH_4}}^{comb} \quad , \tag{8}$$

it is estimated that cumulative mass flow of combustible gases is approximately

$$m_{\mathrm{CH_4}} \sim 0.361 m_v \quad , \tag{9}$$

where $m_v = 0.75\ m_w$. This mass flow is a fuel source for the secondary fire, which appears above the wood samples during the simulations.

From the modelling viewpoint, the overall transfer of mass and momentum from the volatiles to the environment is negligible. It is the subsequent combustion of volatiles that has much larger impact. The main mechanical property of volatiles is their buoyancy in the air, which has been preserved by choosing a single positively buoyant flammable gas (i.e. methane). The energy transfer between wood and the gaseous environment has been implemented through coupling of the convection-diffusion thermal energy equation in the porous solid (4) with the convective, diffusive and radiative heat transfer in the gaseous environment.

The influence of volatiles on the chemical composition is also negligible, as the overall amount of volatiles is small. Even the combustion products arising from the burning volatiles do not have a significant effect on chemical composition nor on thermal radiation transport as the vast majority of the combustion products come from the burning propane fuel.

3.2 Fluid modelling

The mass, momentum and energy transport in gaseous environment is modelled with the Favré-averaged transport equations to better represent turbulence and changes in material composition [21]:

$$\partial_t \rho + \partial_j \left(\rho \bar{v}_j \right) = 0 \tag{10}$$

$$\partial_t \left(\rho \bar{v}_i \right) + \partial_j \left(\rho \bar{v}_j \bar{v}_i \right) = -\partial_i \bar{p} + \partial_j \left(\mu \left(\partial_j \bar{v}_i + \partial_i \bar{v}_j \right) - \frac{2}{3} \mu \left(\partial_l \bar{v}_l \right) \delta_{ji} \right) + g \left(\rho - \rho_{ref} \right) - \partial_j \left(\rho \overline{v_j' v_i'} \right) \tag{11}$$

$$\partial_t \left(\rho \bar{h} \right) - \partial_t \bar{p} + \partial_j \left(\rho \bar{v}_j \bar{h} \right) = \partial_j \left(k \partial_j \bar{T} \right) + \bar{v}_j \partial_j \bar{p} + S_c^{comb} \Delta h_c^{comb} + S^{rad} - \partial_j \left(\rho \overline{v_j' h_j'} \right) \tag{12}$$

where besides the reaction energy release $S_c^{comb} \Delta h_c^{comb}$, the radiation contribution S^{rad} has to be also taken into account.

The gaseous mixture contains components of air (N_2 and O_2), propane (C_3H_8) as a source of primary fire, methane (CH_4) that models the gaseous phase of wood volatiles, and combustion products (CO_2 and H_2O). For the transport of C_3H_8, CH_4, O_2, CO_2 and H_2O, separate mass fraction transport equations are used:

$$\partial_t \left(\rho \bar{\xi}_c \right) + \partial_j \left(\rho \bar{v}_j \bar{\xi}_c \right) = \partial_j \left(\rho D_c \partial_j \bar{\xi}_c \right) + S_c^{comb} - \partial_j \left(\rho \overline{v_j' \xi_c'} \right) \tag{13}$$

where S_c^{comb} is the mass source term due to the chemical reaction involving component *c*. The mass fraction of nitrogen is determined from the condition $\xi_i = 1$. A detailed description of reaction mechanism will be given later in the text.

Turbulence

In the present work, a Shear Stress Transport (SST) model is used to model turbulence. The model was developed by Menter [22] and it is a combination of the *k*-ε model and the *k*-ω model of Wilcox [23], where the turbulence eddy frequency $\omega = \rho k/\mu_t$ is used instead of turbulence dissipation rate ε. The idea behind the SST model is to combine the best elements of the *k*-ε and the *k*-ω model with help of a blending function F_1:

$$F_1 = tanh\left(arg_1^4\right) \tag{14}$$

where $arg_1 = min\left(max\left(\frac{\sqrt{k}}{\beta^* \omega \ell}; \frac{500\mu}{\rho \omega \ell^2} \right); \frac{4\sigma_{\omega 2} \rho k}{CD_{k\omega} \ell^2} \right)$ and $CD_{k\omega} = max\left(\frac{2\sigma_{\omega 2} \rho \partial_j k \partial_j \omega}{\omega}; 10^{-10} \right)$.

The blending function F_1 is 1.0 at a wall and 0.0 far away from a wall, thus activating the Wilcox model in the near-wall region and the *k*-ε model for the rest of the flow:

$$\text{SST model} = F_1 \cdot (k\text{-}\omega \text{ model}) + (1\text{-}F_1) \cdot (\, k\text{-}\varepsilon \text{ model}\,) \tag{15}$$

Combining transport equations of both models by using the scheme (15), the transport equation for turbulence kinetic energy *k* is formulated as

$$\partial_t(\rho k) + \partial_j\left(\rho \bar{v}_j k\right) = \tilde{P} + G + \partial_j\left((\mu + \frac{\mu_t}{\sigma_{k3}}) \partial_j k \right) - \beta^* \rho \omega k \tag{16}$$

where $\tilde{P} = \max(P, 10\beta^* \omega k)$ is the turbulence production term due to normal and shear stresses, which is bounded to prevent build-up of turbulence production in the stagnation regions. The term *G* is the turbulence production due to buoyancy. Furthermore, the transport equation for turbulence eddy frequency ω is defined as

$$\begin{aligned} \partial_t(\rho\omega) + \partial_j\left(\rho \bar{v}_j \omega\right) = & \left(\alpha_3 \rho S^2 + \alpha_3 \frac{\rho}{\mu_t} max(G,0) - \frac{\rho}{\mu_t} G \right) + \partial_j\left((\mu + \frac{\mu_t}{\sigma_{\omega 3}}) \partial_j \omega \right) \\ & + (1 - F_1) \frac{2\rho}{\sigma_{\omega 2}} \partial_j k \partial_j \omega - \beta_3 \rho \omega^2 \end{aligned} \tag{17}$$

With this approach, the attractive near-wall performance of the Wilcox model, which is able to accurately approximate viscous sublayer, is utilised without the potential errors resulting from the free stream sensitivity of that model.

Using the turbulence kinetic energy k and turbulence eddy frequency ω that are calculated from equations (16 & 17), the eddy viscosity μ_t is defined as

$$\mu_t = \rho \frac{\alpha_1 k}{max(\alpha_1 \omega; S F_2)} \tag{18}$$

where $F_2 = tanh\left(arg_2^2\right)$, $arg_2 = max\left(\frac{2\sqrt{k}}{\beta^* \omega \ell}; \frac{500\mu}{\rho \omega \ell^2}\right)$ and S is an invariant of the strain rate.

The values of the parameters β^*, $\sigma_{\omega 2}$, σ_{k3}, α_3, $\sigma_{\omega 3}$, β_3, α_1 and Pr_t , used in the SST model, are in Table 2. Note that the parameters σ_{k3}, α_3, $\sigma_{\omega 3}$ and β_3 are not constant. Their values are calculated locally during a simulation from the values of the k-ω and the k-ε model using the scheme (15).

Table 2: The shear stress transport model parameters

β^*	$\sigma_{\omega 2}$	σ_{k3}	α_3	$\sigma_{\omega 3}$	β_3	α_1	Pr_t
0.09	1.168	2.0-1.0	5/9-0.44	2.0-1.168	0.075-0.0828	0.31	0.9

Finally, using the obtained turbulence viscosity μ_t, Reynolds stresses, heat and mass fluxes are calculated as:

$$\rho\overline{v_j' v_i'} = -\mu_t 2S_{ij} + \frac{2}{3}\rho k \delta_{ij}, \quad \rho\overline{v_j' h'} = -\frac{\mu_t}{Pr_t}\partial_j \bar{h}, \quad \rho\overline{v_j' \xi_c'} = -\frac{\mu_t}{Sc_t}\partial_j \bar{\xi}_c \quad . \tag{19}$$

Thermal radiation

The dominant heat transfer mechanism in the presented case is thermal radiation. In order to determine the radiation source S^{rad} due to volumetric absorption in each control volume as well as the radiation heat fluxes on the walls, the radiation transport is modelled using the Discrete Transport model [24].

Neglecting anisotropic scattering, thermal radiation equation can be simplified to

$$d_s I_\lambda(r,s) = -(K_{a\lambda} + K_{s\lambda}) I_\lambda(r,s) + K_a I_b(\lambda,T) + \frac{K_{s\lambda}}{4\pi} \int_{4\pi} I_\lambda(r,s') d\Omega' \tag{20}$$

The radiation intensity I_λ is then integrated along each ray from the boundaries of simulation domain assuming reasonable homogenous radiation intensity field:

$$I_\lambda(r,s) = I_{0\lambda} e^{-(K_{a\lambda}+K_{s\lambda})s} + I_{b\lambda}\left(1 - e^{-K_a s}\right) + K_{s\lambda}\bar{I}_\lambda \tag{21}$$

The first term represents the contribution due to absorption and out-scattering of the radiation leaving the boundary, the second term the emitted radiation, and the third term the in-scattering in each volume element.

To better represent radiative transport properties of combustion gas mixture, the multigrey gas formulation of Taylor and Foster [25] is used. Radiative properties of the mixture are expressed as a function of temperature and $p \cdot s$, which is the product of the partial pressure and the ray length. This functional dependence can be accurately correlated by assuming that the mixture behaves as a group of a sufficient number of grey gases. Therefore, for each grey gas, the radiation absorption coefficient is calculates as

$$K_{ag} = p\left(k_g\left(\bar{\zeta}_{CO_2} + \bar{\zeta}_{H_2O}\right) + k_{HCg}\left(\bar{\zeta}_{CH_4} + \bar{\zeta}_{C_3H_8}\right)\right) \tag{22}$$

where k_g and k_{HCg} are empirical parameters for a given grey gas (Table 3). They were obtained from the measured spectral data by Hadvig [26] and Beer et al. [27]. Note, that in the presented combustion case, the dominant emitters of radiation are carbon dioxide and water vapour.

In the performed numerical simulations, 4 grey gases are used in the multigrey gas formulation. For each grey gas, equation (21) is solved and partial radiation intensity I_g is obtained. In the same way, the radiation heat fluxes and, consequently, also the radiation source terms in the energy equation (12) are calculated for each gas separately:

$$q_{g,i}^{rad} = \int_{4\pi} I_g(r,s)\cos\varphi_i \cos\theta \, d\Omega \tag{23}$$

$$S_g^{rad} = -\partial_i q_{g,i}^{rad} \tag{24}$$

The resulting radiation heat fluxes are obtained by a weighted sum:

$$q_i^{rad} = \sum_{g=1}^{4} a_g q_{g,i}^{rad} \tag{25}$$

where the coefficients a_g are represented as linear functions of temperature:

$$a_g = b_{1g} + 10^{-5} b_{2g} \overline{T} \tag{26}$$

The values of grey gas parameters b_{1g} and b_{2g} for the present case are given Table 3.

Table 3: Gray parameters for $p_{H_2O} / p_{CO_2} = 1$

gas	k_g [m^{-1} atm^{-1}]	k_{HCg} [m^{-1} atm^{-1}]	b_{1g} [-]	b_{2g} [K^{-1}]
1	0.0	3.41	0.4092	7.53E-05
2	0.91	0.0	0.284	2.58E-05
3	9.4	0.0	0.211	-6.54E-05
4	130.0	0.0	0.0958	-3.57E-05

Combustion process

The chemical reaction between the fuel of the primary fire (propane) and air is modelled with a single step chemical reaction:

$$C_3H_8 + 5\left(O_2 + \frac{0.79}{0.21}N_2\right) \Rightarrow 3CO_2 + 4H_2O + 5\frac{0.79}{0.21}N_2 + \Delta h^{comb}_{C_3H_8} \ . \quad (27)$$

where $\Delta h^{comb}_{C_3H_8}$ = 2044.2 kJ/mol is the combustion heat release. Also, combustion of the gaseous phase of the pyrolysis volatiles (methane) is described with a single step chemical reaction:

$$CH_4 + 2\left(O_2 + \frac{0.79}{0.21}N_2\right) \Rightarrow CO_2 + 2H_2O + 2\frac{0.79}{0.21}N_2 + \Delta h^{comb}_{CH_4} \ . \quad (28)$$

where $\Delta h^{comb}_{CH_4}$ = 802.35 kJ/mol is the combustion heat release.

The reaction rate of these reactions is calculated with the eddy-dissipation model [28]. This model has been widely used and validated in the past for a numerous different fire cases. A selection of publications on the topic is publicly available at [29].

The eddy-dissipation model is based on the assumption that a chemical reaction is fast relative to the transport processes in the flow. The model assumes that the reaction rate may be related directly to the time required to mix reactants at the molecular level. Therefore, the level of turbulent mixing, which is defined with turbulence time scale $t_{flow} = k/\varepsilon$, is a controlling condition for a combustion reaction. The other limiting factor of the combustion reaction is the availability of fuel and oxygen.

Thus, the following mathematical description of the reaction rates is used for the propane and the methane combustion:

$$R_{C_3H_8}^{comb} = C_A \frac{\varepsilon}{k} min\left(\frac{\overline{\zeta}_{C_3H_8}}{\nu'_{C_3H_8}}, \frac{\overline{\zeta}_{O_2}}{\nu'_{O_2}} \right) \tag{29}$$

and

$$R_{CH_4}^{comb} = C_A \frac{\varepsilon}{k} min\left(\frac{\overline{\zeta}_{CH_4}}{\nu'_{CH_4}}, \frac{\overline{\zeta}_{O_2}}{\nu'_{O_2}} \right) \tag{30}$$

where C_A = 4.0 is the empirical constant. The mass source term in the species transport equation (13) is then calculated as

$$S_c^{comb} = M_c \left(\nu''_c - \nu'_c \right) R^{comb} \tag{31}$$

where ν'_c and ν''_c are stoichiometric coefficients of the reactants and the products.

The described modelling of the combustion process is idealized, which means that many processes (e.g. soot formation, change of surface radiation properties) that do occur are not taken into account or they are significantly simplified. These modelling simplifications are somehow justified for the present experimental setup, where dried beech wood has been selected for the solid combustible targets and propane for the burner fuel in order to avoid influence of moisture on the combustion process and to minimise soot production. This is significantly different than in a real flashover event, where a lot of different combustible materials produce a lot of soot.

In the experiments, the soot production due to combustion of the propane fuel in a well ventilated environment is not of significant importance. Also, the soot production of most of the pyrolysis volatiles (H_2, CO, CH_4) is small. More significant impact may have tar decomposition and higher hydro-carbons, which is not taken into account.

4 Boundary and initial conditions

The fuel inlet at the top of the burner is represented with a boundary mass source that provides a constant propane flow rate of 1.2 g/s. The temperature of the incoming mass flow is approximated with the arithmetic average of the wall temperature and the ambient temperature of 20^{o}C. The correct estimate of the inflow temperature is important as propane is denser than air. Prescribing the temperature that is too low would result in a negatively buoyant jet with completely different dynamics.

Although, the hood plays an important role in formation of the hot gaseous upper layer, it is modelled with a single thin surface, where a constant heat transfer coefficient is prescribed. The heat transfer coefficient is estimated from thermal conductivity and thickness of the insulation layer between the inner and the outer hood:

$$\alpha_{hood} \sim \frac{k_{insul}}{\delta_{insul}} = 7.7 \frac{W}{m^2 K} \ , \tag{32}$$

For the rest of wall boundaries, no-slip and adiabatic boundary conditions are prescribed.

At the outermost boundaries of the domain, "opening" boundary conditions are assigned. The opening boundary conditions allow the fluid to cross the boundary in both directions by setting static pressure p_{stat} for the outgoing flow, and total pressure $p_{stat} + 0.5\rho v^2$ for the incoming flow.

All the walls in the simulation domain are considered opaque and diffusive with total emissivity ε = 1.0. An exception are wooden surfaces, where total emissivity gradually changes during pyrolysis from 0.6 to 1.0 [19].

The initial conditions for the numerical simulations represent the state before the start of fuel inflow and combustion. Therefore, the fluid in the simulation domain consists initially of air ($\psi_{O_2} = 0.21$ and $\psi_{N_2} = 0.79$) with zero velocity field. In the solid blocks, the initial value of progress variable α is set to 1.0. The initial temperature in fluid as well as in solid blocks is 20^{o}C.

5 Computational implementation

The geometrical and physical model of flashover was solved using the ANSYS CFX software (ver. 10.0). The CFX code solves the system of Navier-Stokes equations on an unstructured numerical grid by implementing the Rhie-Chow interpolation scheme [30] between pressure and mass fluxes. The numerical methods implemented by the code are described in details in the ANSYS CFX-Solver Theory Guide [21] and therefore will not be repeated here. The exceptions are the information particular to the presented case.

To perform the numerical simulation for the presented geometrical arrangement, an unstructured computational mesh with 253,959 grid nodes and 1,099,986 elements was generated for the gaseous part of the simulation domain. The majority of elements were tetrahedra, with slowly inflating layers of prisms aligned with the walls. The inflation layers are necessary to capture momentum and thermal boundary layer effects. Additionally, a mesh with 3,367 grid nodes and 5,424 hexahedral elements was generated for each of the three wood samples.

A constant timestep of 0.04 s was used as the best balance between the accuracy of the numerical results and computational costs. A total of 12,500 of integration timesteps were needed to simulate 500 s of the flashover experiment.

6 Results and discussion

At the start of the numerical simulation, a jet of propane is ignited and a mixture of hot gases that mostly contains combustion products starts to fill the hood above the burner. After the initial 10 s, the flame and the hot layer stabilize. They represent a constant source of thermal radiation that heats the upper surface of the wood samples.

Figure 4 shows convective and irradiation heat flux at the top surface of the wood samples. After the initial transient, when the hot layer stabilizes, the incoming heat flux reaches values between 20 and 30 kW/m^2, being higher for the wood surfaces that are closer to the burner. With the ignition of volatile pyrolysis products, the heat flux increases by approx. 12 kW/m^2. This rapid heat flux increase that marks the ignition event shows that the ignition time is different for each wood sample.

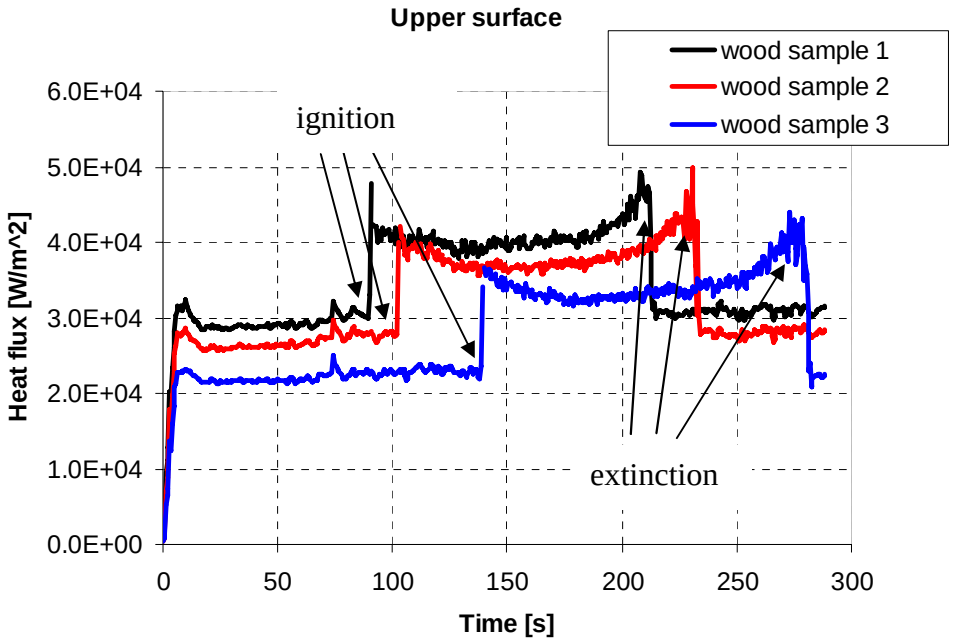

Figure 4: Wall convective and irradiation heat fluxes ($q_c + q_i$) at the top of wood samples

Due to combustion of volatiles above the wood samples, the heat flux stays elevated until the fuel (wood) is consumed. The time of extinction is different for each block, as well as the duration of wood degradation. After the extinction, the heat flux decreases to the values before the ignition.

Figure 5 shows computed mass flow of combustible volatiles from the wood samples. At the beginning of the simulation, the mass flow is negligible as the wood particles needs to be preheated to approximately 650 K. With gradual change of thermal radiation properties of the wood upper surfaces, larger proportion of irradiated heat flow is absorbed. This causes an increase in the rate of heating of the wood and in rate of the release of combustible volatiles. With the ignition of the volatiles, the release process is further accelerated as the irradiation heat flux, due to proximity of the secondary fire, increases (approx. 12 kW/m^2).

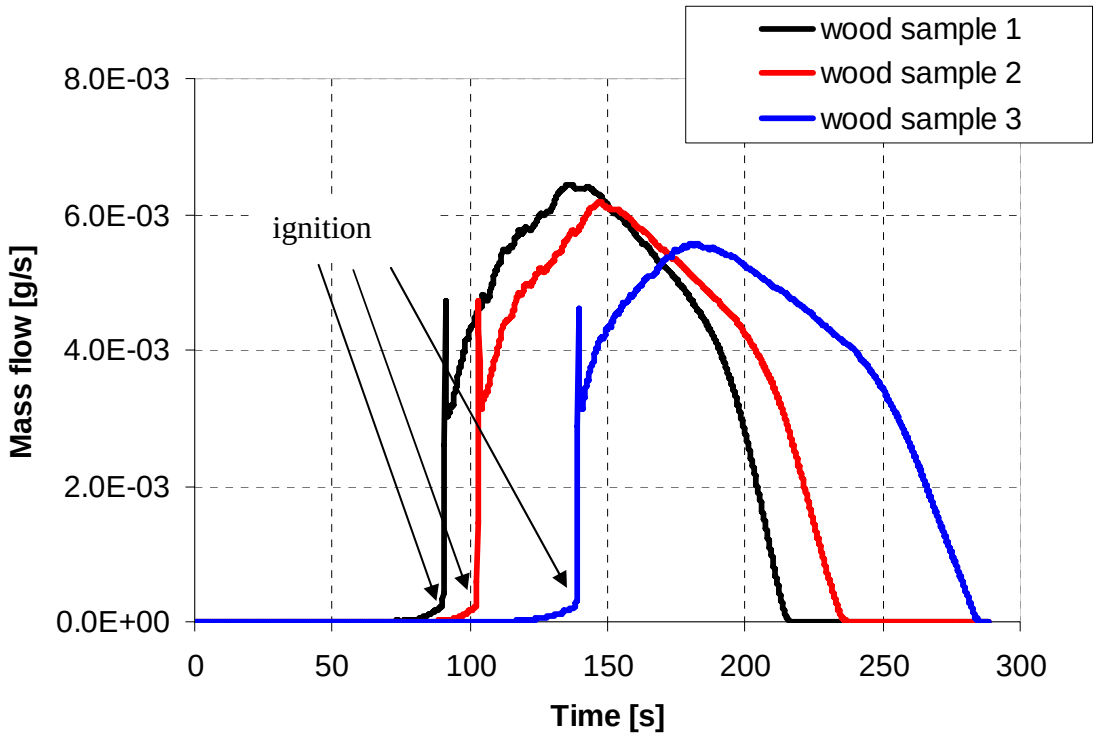

Figure 5: Mass flow of combustible volatiles at the top of wood samples

Figures 6 (a – c) present the temperature field above the three wood samples after the ignition of volatile pyrolysis products at 95 s, 120 s and 160 s, respectively. As such, Fig. 6a shows the fire above the wood sample 1, Fig. 6b above the samples 1 and 2, and Fig. 6c above all three samples. The presented temperature field also clearly shows the separation of the flow into the hot upper layer, where combustion products accumulate in the hood, and the colder lower layer with entrainment of the surrounding air.

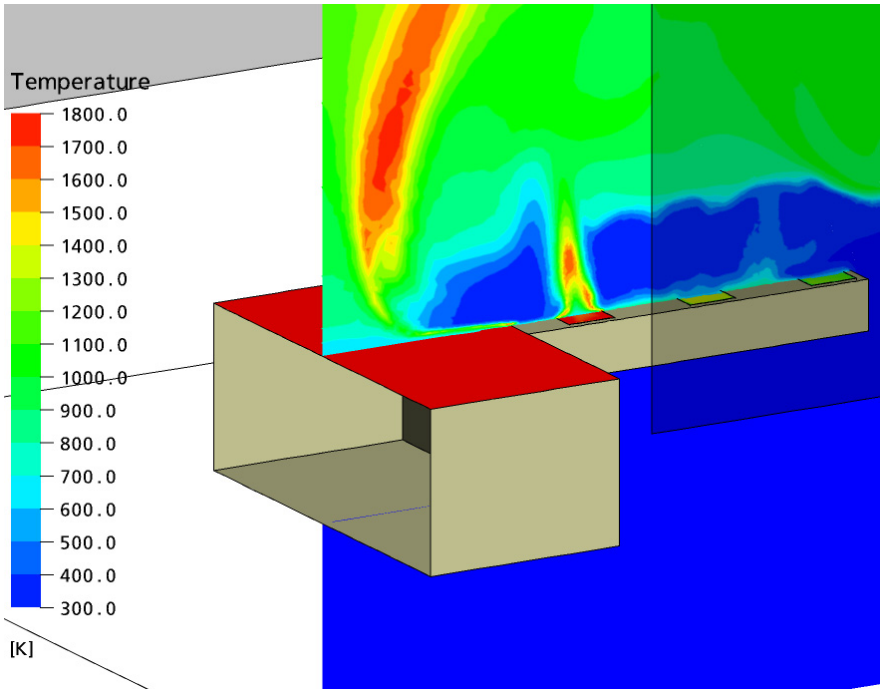
Temperature
1800.0
1700.0
1600.0
1500.0
1400.0
1300.0
1200.0
1100.0
1000.0
900.0
800.0
700.0
600.0
500.0
400.0
300.0
[K]

a)

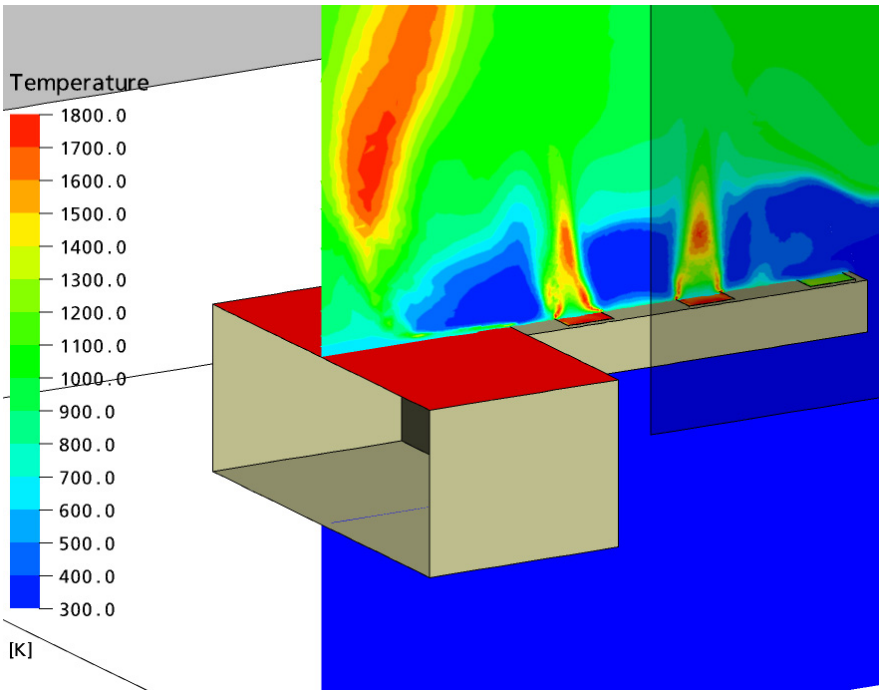
Temperature
1800.0
1700.0
1600.0
1500.0
1400.0
1300.0
1200.0
1100.0
1000.0
900.0
800.0
700.0
600.0
500.0
400.0
300.0
[K]

b)

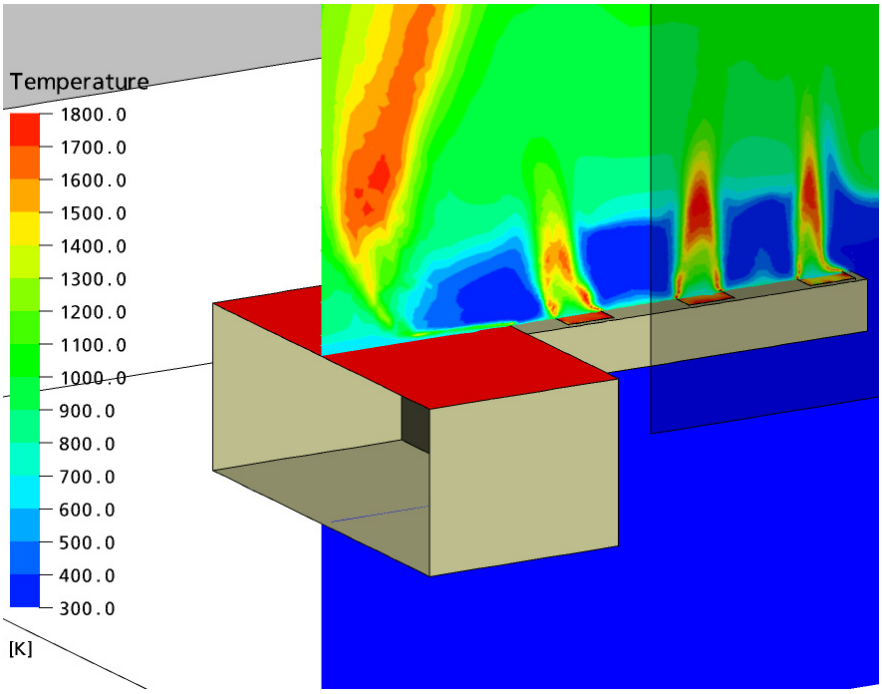

c)

Figure 6: Temperature field cross section: **a)** at 95 s - after ignition of the first wood sample, **b)** at 120 s - after ignition of the second wood sample, and **c)** at 160 s - after ignition of the third wood sample

The temperature was recorded at the initial location of the upper surface of the wood samples, which is exposed to convective and irradiation heat flux, and at the lower surface, which is embedded in the insulation.

Figure 7a shows the temperature at the upper surface of all the three wood samples. At the beginning, the temperature increases in a slightly parabolic manner following by a rapid increase due to the ignition of pyrolysis volatiles. After the ignition event, the temperature increases with the same rate as before the ignition. The end of wood degradation is marked with rapid acceleration of pyrolysis as the wood samples become practically isothermal.

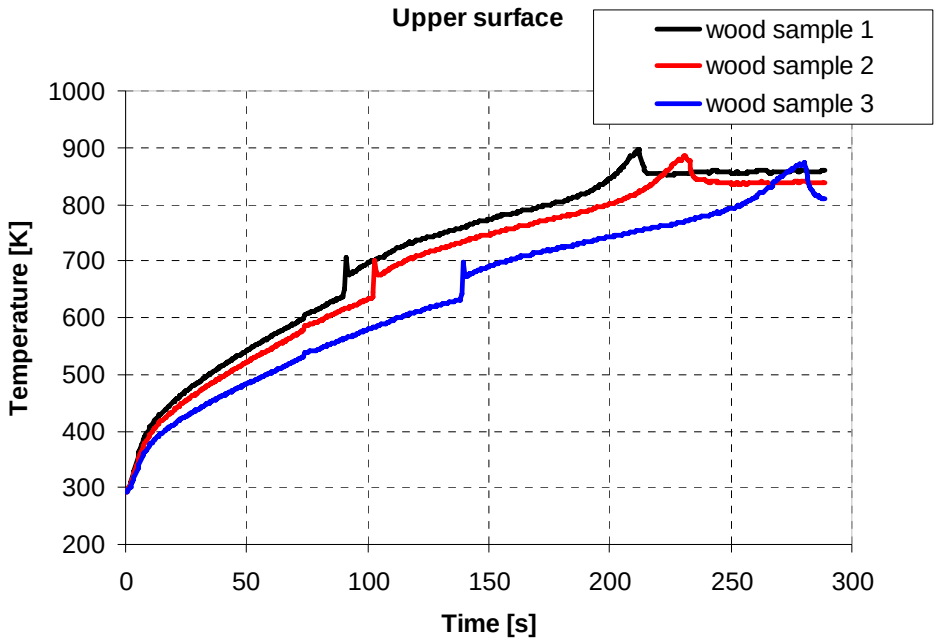

a)

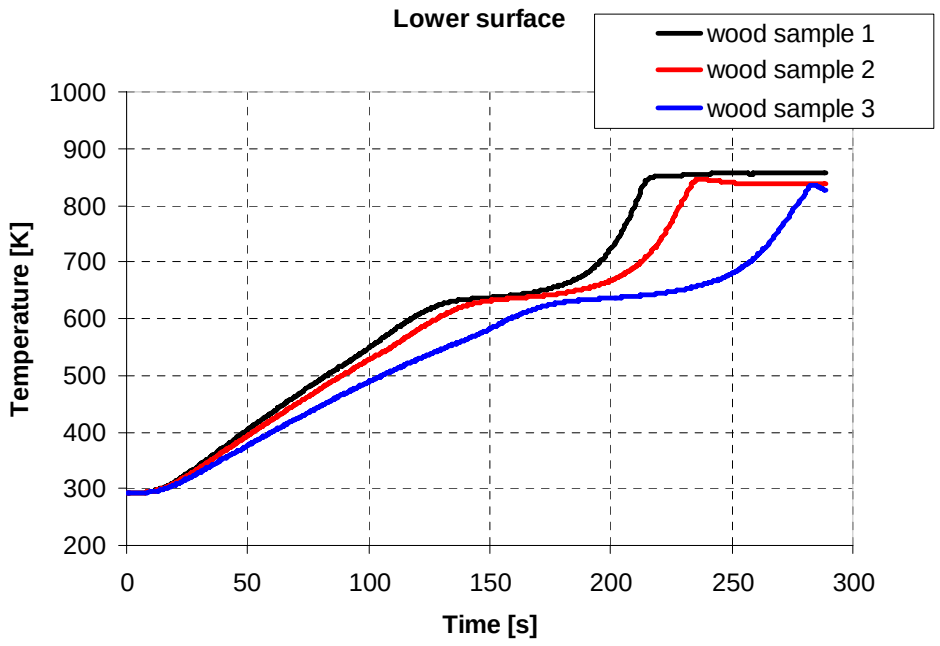

b)

Figure 7: Temperature variations: **a)** at the upper surface, **b)** at the lower surface of the wood samples

The temperature at the lower surface increases at almost the same rate as at the upper surface (Figure 7b), but with a certain delay as a result of energy diffusion from the upper to the lower surface.

The period of wood degradation is different for each sample as it depends on the amount of received heat. Figure 4 showed that the incoming (convective and irradiation) heat flux is the highest on the wood sample that is the closest to the propane burner.

To validate the described simulation approach, the calculated ignition time was compared with the experimental observations [17]. The ignition times for five experimental tests and for the numerical simulation are given in Table 4.

Table 4: Comparison of ignition times

	Ignition times [s]		
	Sample 1 (170 mm)	Sample 2 (250 mm)	Sample 3 (330 mm)
Test A	107	244	361
Test B	121	166	293
Test C	94	204	282
Test D	95	154	269
Test E	138	222	327
Numerical simulation	91	103	140

The ignition time for the first wood sample that is the nearest to the propane burner shows a good agreement with the experimentally obtained values, whereas the ignition times for the second and the third sample show increasing differences.

During the experiments, temperature was recorded at the upper surfaces of the three wood samples. Figures 8 show comparison of calculated and measured temperature variations. The

calculated temperature variation for the first wood sample (Fig, 8a) matches well the experimentally obtained values over the whole simulation time. However, the time variations of the temperature for the second and the third wood sample (Figs. 8b and 8c) show that the model overpredicts the temperature from the beginning of the simulation, which leads to the premature ignition of the wood samples.

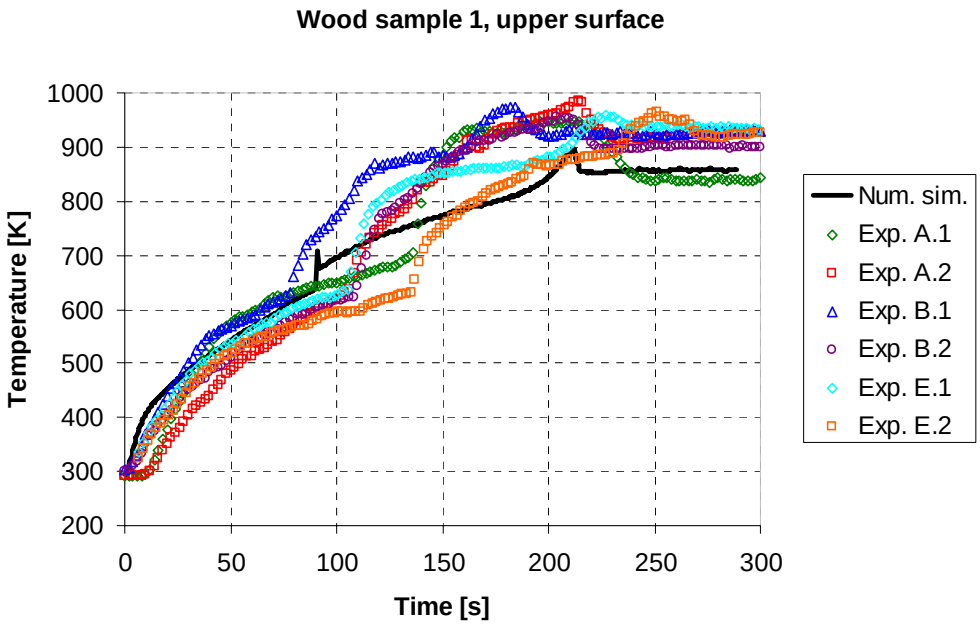

a)

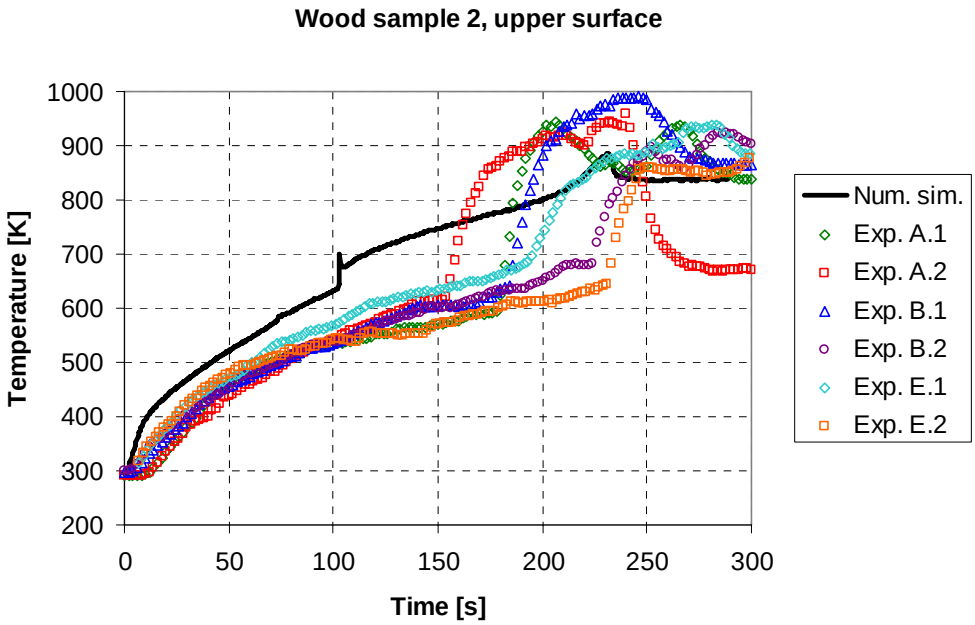

b)

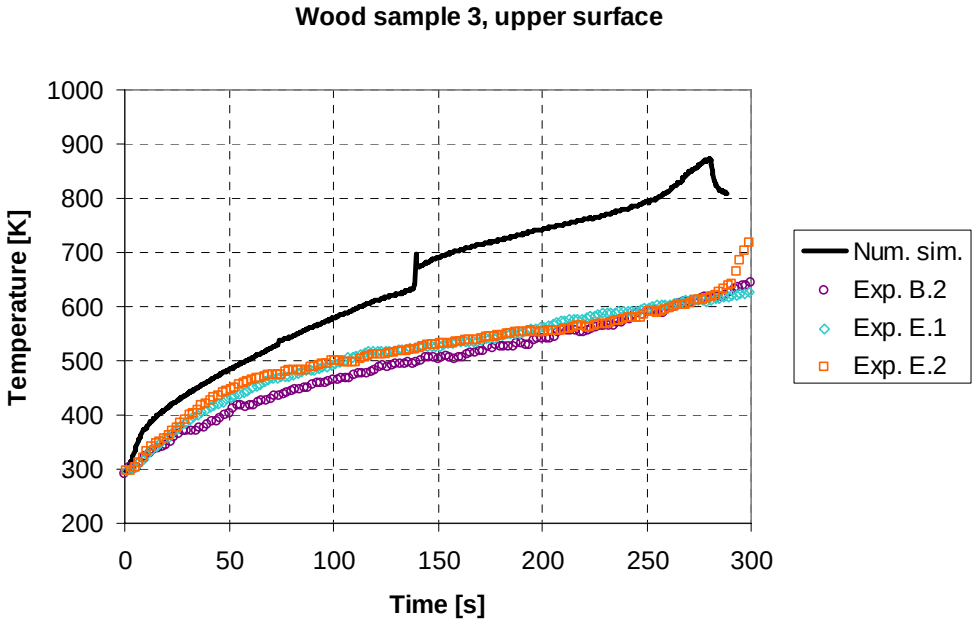

c)

Figure 8: Comparison of temperature variations at the upper surface of the wood samples: **a)** sample 1, **b)** sample 2, and **c)** sample 3

In our opinion, the discrepancy between the experimentally obtained and the simulated ignition times, especially for the third wood sample, is a consequence of modelling

simplifications. Reducing the model complexity by describing the double-walled hood as a single wall with a heat transfer coefficient, inadequately models the heat transfer from the hot layer of gases to the environment. As a result, the calculated temperature of the hot gas layer is overestimated and, therefore, emits stronger thermal radiation.

7 Conclusions

For prediction of the flashover phenomena, a CFD model was built that closely follows the experimental setup at CNRS-ENSMA-Poitiers [17]. The primary source of fire was a propane burner with thermal power of 55 kW. Square beech wood samples with the edge length of 30 mm and 5 mm thickness were used as fire spread targets. Exposed to the heat fluxes from the fire, the temperature in the wood samples rises; at some stage the wood undergoes pyrolysis. In the numerical model, the pyrolysis front was tracked with a progress variable that defines a solid mixture of virgin wood and char. The total heat release rate of wood volatiles was approximated with an equivalent mass flow of methane.

The Shear Stress Transport (SST) model was used to describe the turbulence of the flow. The combustion reaction between the propane introduced by the burner and the surrounding air was modelled as a single step chemical reaction. Also, the reaction between the methane and the air was described in the same way. The combustion reaction rate was calculated with the eddy-dissipation model. An important heat transfer mechanism in the presented case is thermal radiation. The radiation transport was calculated using the Discrete Transport model with the multigrey gas formulation.

To verify the developed model, a numerical simulation of the flashover experiment was performed. The collected results gave a qualitative insight into the radiation induced ignition

and fire spread over solid surfaces. It also helped us to identify important parameters of the flashover phenomenon and to evaluate their influence.

The results show that after the initial transient, the flow field stabilizes, forming a cold and a hot horizontal layer of gases. The ignition of the wood samples is triggered at the upper surface when its temperature reaches approx. 650 K. At this point the secondary flame appears which further raises temperature in the wood samples and accelerates pyrolysis. As each wood sample is exposed to a different incident heat flux, large differences in ignition times are observed in the experiments and confirmed with the numerical simulation. Consequently, the time of degradation of the most exposed wood sample, 0.17 m away from the burner, is approx. 15% shorter than of the most distant wood sample.

The comparison of the calculated and the experimentally measured ignition times shows a good agreement that is well inside experimental variability for the first wood sample (0.17 m). It was calculated that the ignition occurs at 91 s, whereas the average measured ignition time is 111 s. For the second and the third wood sample, the calculated ignition time is shorter than the experimentally observed. Also the calculated temperature time variation at the upper surface of the first wood sample matches the experimental data well, but the differences are larger for the second and the third sample. We believe that these ignition time discrepancies are mostly the consequence of the hood model simplification, which results in higher temperatures of the combustion products trapped under the hood. It is important to mention that the composition (i.e. flammability range) and thermal requirements for ignition were also not taken into account. They would delay the ignition of the wood targets and slow the combustion of volatiles. This needs to be further investigated in the future.

Acknowledgments

The present work was performed as a part of the project "Under-Ventilated Compartments Fires (FIRENET)" (Co. No. HPRN-CT-2002-00197). The project was supported by the EU Research Training Network FP5, which is gratefully acknowledged.

References

1. Drysdale, D., An Introduction to Fire Dynamics, John Wiley & Sons, 1990.
2. Di Blasi, C., Physico-Chemical Processes Occurring Inside a Degrading Two-Dimensional Anisotropic Porous Medium, Int. J. Heat Mass Transfer, 1998, 41, pp. 4139-4150.
3. Karlsson, B., Quintiere, J.G., Enclosure Fire Dynamics, CRC Press, Boca Raton, USA, 2000.
4. Spearpoint, M.J., Mowrer, F.W., McGrattan, K.B., Simulation of a Compartment Flashover Fire Using Hand Calculations, Zone Models and a Field Model, Int. Conf. on Fire Research and Engineering (ICFRE3), Oct. 4-8, 1999, Chicago, IL, USA, Proceedings, pp. 3-14.
5. Peacock, R.D., Reneke, P.A., Bukowski, R.W., Babrauskas, V., Defining Flashover for Fire Hazard Calculations, Fire Safety J., 1999, Vol. 32, pp. 331-345.
6. Grosshandler, W. L., Role of Science and Engineering in Reducing Fire Risk, Fire Risk and Hazard Assessment Research Application Symposium, July 9-11, 2003, Baltimore, USA, Proceedings, pp. 1-21.
7. Babrauskas, V., Peacock, R. D., Reneke, P. A., Defining Flashover for Fire Hazard Calculations. Part 2, Fire Safety J., 2003, Vol. 38, pp. 613-622.

8. White, N., Dowling, V., Barnett, J., Full-Scale Fire Experiment on a Typical Passenger Train, The 8th Sym. of the Int. Assoc. of Fire Safety Science, Sept. 18–23, 2005, Beijing, China, Proceedings, Paper 112.
9. Luo, M., He, Y., Beck, V., Application of Field Model and Two-Zone Model to Flashover Fires in a Full-Scale Multi-Room Single Level Building, Fire Safety J., 1997, Vol. 29, pp. 1 -25.
10. Chow, W.K., Predictability of Flashover by Zone Models, J. Fire Sciences, 1998, Vol. 16, No. 5, pp. 335-350.
11. Novozhilov, V., Flashover Control under Fire Suppression Conditions, Fire Safety J., 2001, Vol. 36, pp. 641-660.
12. Atreya, A., Pyrolysis, Ignition and Fire Spread on Horizontal Surfaces of Wood, Ph.D. Thesis, 1983, Harvard University, Cambridge, MA, USA.
13. Fredland, B., A Model for Heat and Mass Transfer in Timber Structures During Fire: A Theoretical, Numerical and Experimental Study, Ph.D. Thesis, 1988, Dept. of Fire Safety Engineering, Lund Institute of Science and Technology, Sweden.
14. Aksit, M., Moss, J.B., Rubini, P.A., Field Modelling of Surface Flame Spread over Charring Materials, Interflam '01, Sept. 17-19, 2001, Edinburgh, Scotland, Proceedings, pp. 1459-1464.
15. Madrzykowski, D., Bryner, N.P., Grosshandler, W.L., Stroup, D.W., Fire Spread Through a Room With Polyurethane Foam Covered Walls, Interflam '04, July 5-7, 2004, Edinburgh, Scotland, Proceedings, Vol. 2, pp. 1127-1138.
16. Edwards, J.C., Hwang, C.C., CFD Modeling of Fire Spread Along Combustibles in a Mine Entry, The 2006 SME Annual Meeting and Exhibit, 2006, March 27-29, St. Louis, Missouri, USA, Proceedigs, No. 06-027.

17. Pearson, A., Most, J.-M., Data on Flashover, Report, June 2006, CNRS, University of Poitiers, ENSMA, Laboratoire de Combustion et de Détonique, UPR 9028, Poitiers, France.
18. Novozhilov, V., Moghtaderi, B., Fletcher, D.F., Kent, J.H., Computational Fluid Dynamics Modelling of Wood Combustion, Fire Safety J., 1996, 27, pp. 69-84.
19. Di Blasi, C., Branca, C., Santoro, A., Hernandez, E.G., Pyrolytic Behavior and Products of Some Wood Varieties, Comb. and Flame, 2001, 124, pp. 165-177.
20. Robert, A.F., Calorific Values of Partially Decomposed Wood Samples, Combustion and Flame, 1964, Vol. 8, pp. 345-346.
21. ANSYS CFX - Solver Theory Guide, Basic Solver Capability Theory, Governing Equations, pp. 22.
22. Menter, F.R., Two-Equation Eddy-Viscosity Turbulence Models for Engineering Applications, AIAA Journal, 1994, Vol. 32, No. 8.
23. Wilcox, D.C., Reassessment of the Scale-Determining Equation, AIAA Journal, 1988, Vol. 26, No. 11, pp. 1299-1310.
24. Shah, N.G., New Method of Computation of Radiant Heat Transfer in Combustion Chambers, Ph.D. thesis, 1979, Imperial College, London, United Kingdom.
25. Taylor, P.B., Foster, P.J., The Total Emissivities of Luminous and Non-Luminous Flames, Int. J. Heat Mass Transfer, 1974, Vol. 17, pp. 1591-1605.
26. Hadvig, S., Gas Emissivity and Absorptivity, J. Inst. Fuel, 1970, Vol. 43, pp. 129-135.
27. Beer, J.M., Foster, P.J., Siddall, R.G., Calculation Methods of Radiative Heat Transfer, HTFS Design Report No. 22, 1971, AEA Technology, UK.
28. Magnussen, B. F., Hjertager, B. H., On Mathematical Modeling of Turbulent Combustion with Special Emphasis on Soot Formation and Combustion, The 16th Symp. (Int.) on Combustion, 1976, Proceedings, pp. 719–729.
29. http://folk.ntnu.no/ivarse/edc/.

30. Rhie, C.M., Chow, W.L., A Numerical Study of the Turbulent Flow Past an Isolated Airfoil with Trailing Edge Separation, AIAA Paper 82-0998, 1982.